A Regional multi-Air Pollutant Assimilation System (RAPAS v1.0) for emission estimates: system development and application

Shuzhuang Feng[1], Fei Jiang[1,2], Zheng Wu[3], Hengmao Wang[1,2], Wei He[1], Yang Shen[1], Lingyu Zhang[1], Yanhua Zheng[1], Chenxi Lou[1], Ziqiang Jiang[4], Weimin Ju[1,2]

[1] *Jiangsu Provincial Key Laboratory of Geographic Information Science and Technology, International Institute for Earth System Science, Nanjing University, Nanjing, 210023, China*

[2] *Jiangsu Center for Collaborative Innovation in Geographical Information Resource Development and Application, Nanjing, 210023, China*

[3] *Chongqing Institute of Meteorological Sciences, Chongqing, 401147, China*

[4] *Jiangsu Environmental Monitoring Center, Nanjing, 210019, China*

Correspondence to: Fei Jiang (jiangf@nju.edu.cn)

Text S1

Figure S1 shows the analysis increments (assimilation minus control) of the 6 species averaged over all initializations. It could be found that the impact of 3DVAR is not only concentrated around the measurement sites, but also transported to downwind areas as discussed in Feng et al. (2018). The longer a species lives, the farther the assimilation benefits are transmitted (e.g., CO). The positive (negative) increments indicate underestimated (overestimated) emissions in local or upwind areas. Specifically, the positive increments of CO and PMC are generally distributed nationwide, especially in the northern part of China, indicating that the emissions of CO and PMC over the whole mainland China were estimated, which may be related to the underestimated residential sources (e.g., coal heating) (Zhi et al., 2017) and local dust caused by higher wind speeds, respectively. For SO_2, NO_2 and $PM_{2.5}$, the negative increments are mainly located in the North China Plain (NCP), the Yangtze River Delta (YRD), and the Sichuan Basin (SCB), as well as Central China, and the significant positive increments mainly correspond with resource-abundant northern regions (e.g., Northeast China, Northwest China, etc.). The increments of $PM_{2.5}$ are related not only to inaccurate emissions but also to the concentration biases of its precursor, which can affect the biases of $PM_{2.5}$ in downwind areas to some extent. The increments of O_3 are negatively correlated with those of NO_2 in terms of their spatial distribution because of strong NO-titration during the winter (Huang et al., 2020; Shi and Brasseur, 2020).

Text S2

Figure S2 shows the time series of the observed daily concentrations in the independent sites and the corresponding simulated ones in the CEP and VEP experiments. Meanwhile, the time series of daily RMSEs are also shown in Fig. S2. Clearly, the concentrations simulated using the posterior emissions are more consistent with the observations. The temporal variation of pollution concentrations is well grasped in the VEPs, even in the heavy pollution stage (16-21 December). Noticeable discrepancies in the simulated CO and PMC between the two experiments are related to the increase in their emissions across mainland China. Benefitting from greater uncertainty settings, rapid convergence of CO and PMC can be found in the first few windows. Similarly, the VEPs show lower RMSEs than those of CEPs throughout the study period.

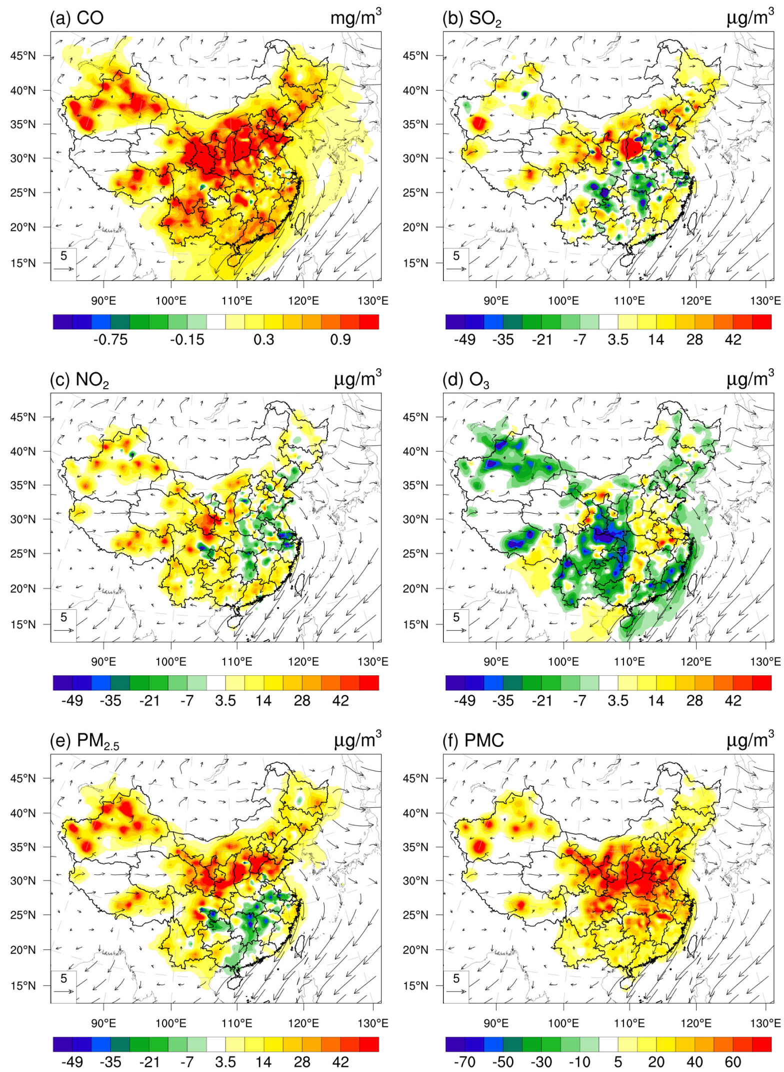

Figure S1. Mean differences of the background and analysis fields of (a) CO, (b) SO_2, (C) NO_2, (d) O_3, (e) $PM_{2.5}$ and (f) PMC at the lowest model level (analysis fields minus background fields). All data are averaged using the fields at 0000, 0600, 1200, and 1800 UTC during the period of 27 to 01 December, 2016.

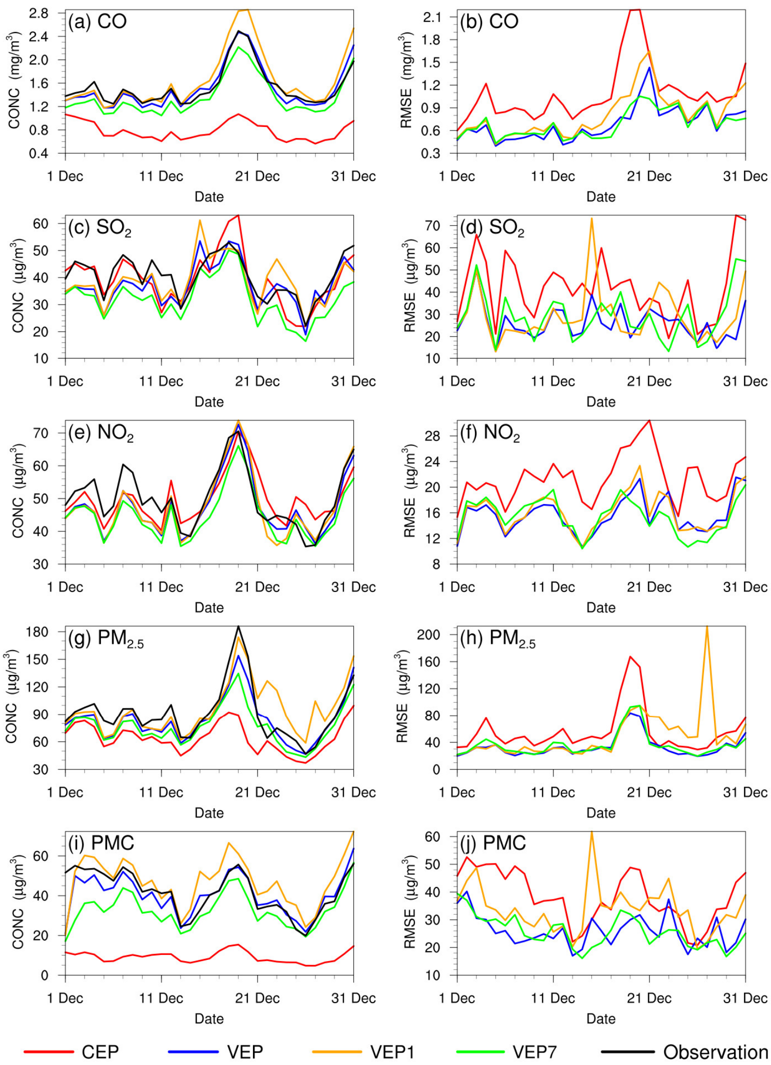

Figure S2. Time series of the daily concentrations (CONC, left, μg m^{-3}) and root mean square error (RMSE, right, μg m^{-3}) obtained from CEP, VEP, VEP1, and VEP2. The simulations were verified against the independent sites.

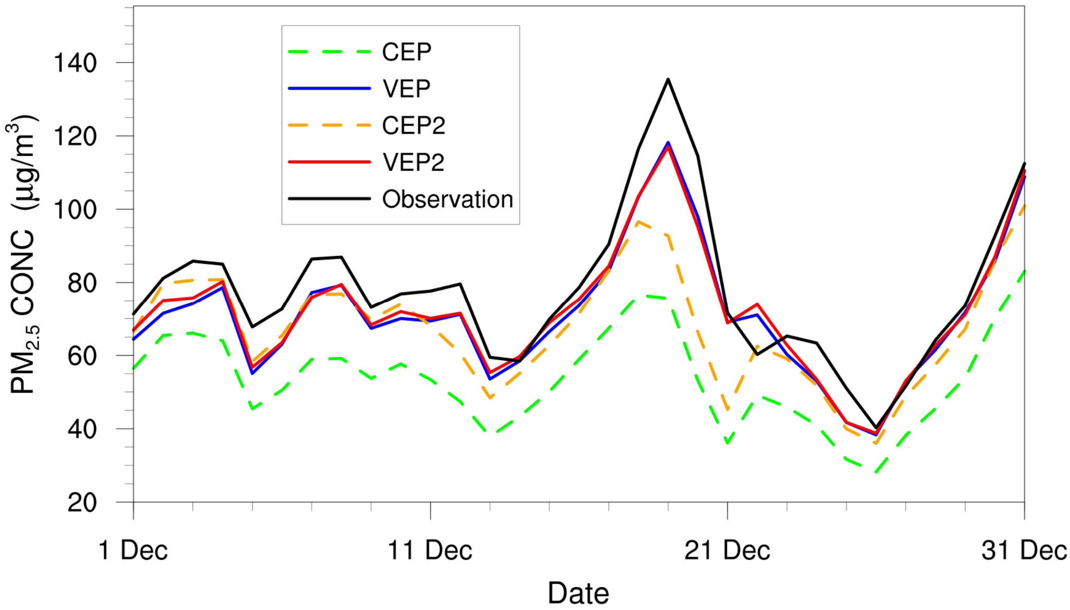

Figure S3. Time series of the daily $PM_{2.5}$ concentrations (CONC, μg m^{-3}) averaged over the whole domain obtained from the observations and simulations. CEP2 and VEP2 represent simulations using prior emissions taken from MEIC 2012 and posterior emissions inferred by EMS2 experiment, respectively.

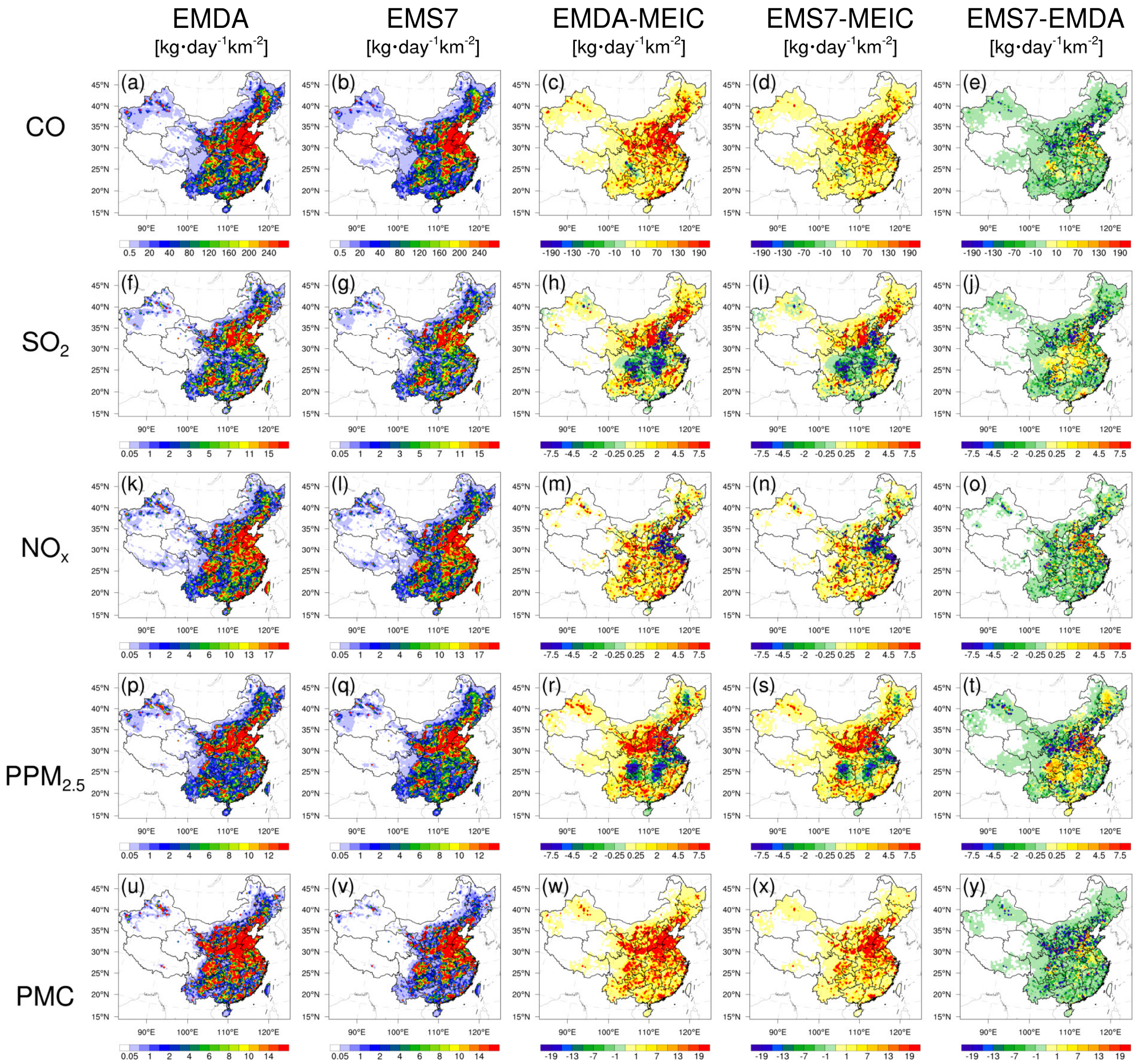

Figure S4. Spatial distribution of the time-averaged posterior emissions of EMDA and EMS7, and differences among prior emissions (MEIC) and posterior emissions of EMDA and EMS7.

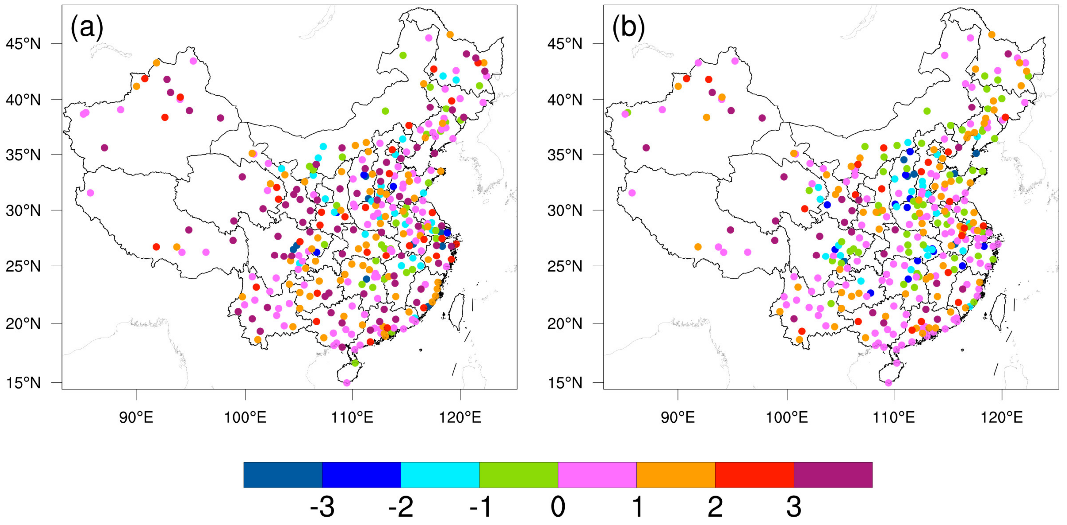

Figure S5. Changes of the (a) BIAS (μg m^{-3}) and (b) RMSE (μg m^{-3}) of the simulated NO_2 between VEP and VEP7 experiments.

Table S1. Estimation of posterior emissions (kton/day) and relative changes (%) compared to prior emissions in each province and the whole mainland China.

Region	CO		SO_2		NO_X		$PPM_{2.5}$		PMC	
	Post.	Diff.	Post.	Diff.	Post.	Diff.	Post.	Diff.	Post.	Diff.
Mainland	1141.9	129.4	54.7	19.7	69.4	5.1	55.4	95.4	97.6	1044.8
Shanghai	4.75	12.5	0.25	-59.5	0.74	-44.0	0.11	-40.8	0.22	249.1
Jiangsu	37.27	30.9	1.10	-23.9	2.90	-38.6	0.96	-34.3	2.46	529.6
Zhejiang	20.15	80.3	0.59	-30.0	2.68	1.9	0.86	77.9	2.15	876.9
Anhui	32.88	69.6	0.79	21.3	2.79	1.5	1.28	-3.0	2.50	495.6
Shandong	93.11	115.9	3.33	-17.5	4.26	-32.7	3.07	19.3	6.11	742.6
Beijing	6.34	108.4	0.06	-15.7	0.35	22.0	0.23	80.7	0.19	544.3
Tianjin	13.40	372.2	0.11	-33.6	0.59	53.3	0.23	73.7	0.35	933.0
Hebei	125.45	158.4	3.47	10.9	5.49	1.1	6.00	176.3	8.23	1176.7
Shanxi	82.17	210.9	9.93	86.9	2.88	-15.4	5.66	236.1	7.20	1274.8
Neimenggu	59.12	231.2	5.48	135.8	3.92	29.0	2.73	163.7	7.11	2144.3
Henan	69.99	120.2	1.14	-39.6	3.09	-22.7	3.05	66.6	6.26	1008.4
Hunan	40.59	56.8	1.52	-40.3	2.36	-5.2	0.69	-52.9	2.98	481.5
Hubei	38.80	73.1	0.57	-76.5	2.27	-1.9	1.17	-12.1	2.32	498.7
Jiangxi	28.71	112.3	1.63	83.0	1.78	19.0	1.52	110.3	2.65	777.5
Guangdong	52.97	175.3	1.19	-32.7	4.66	31.1	1.91	89.4	2.65	565.6
Guangxi	24.81	120.8	1.18	-1.5	2.30	52.2	1.70	103.6	1.75	512.5
Fujian	12.22	113.8	0.81	60.3	1.91	57.8	0.75	99.0	1.35	904.3
Hainan	1.94	20.5	0.14	-10.0	0.31	6.6	0.09	-17.0	0.07	106.9
Liaoning	49.69	175.2	4.04	178.8	2.71	-5.9	1.99	94.7	3.93	1377.3
Heilongjiang	38.64	90.2	1.10	25.7	1.82	-2.6	1.40	25.6	0.99	345.6
Jilin	35.61	176.2	3.36	376.2	2.46	69.2	1.72	132.1	0.87	437.8
Shaanxi	49.30	212.9	1.62	-9.5	2.40	37.7	3.64	294.2	7.25	2750.2
Gansu	49.41	423.7	1.51	118.6	1.97	100.1	3.27	521.4	9.64	8264.2
Xinjiang	39.94	383.4	1.48	21.0	2.69	48.2	4.29	720.3	2.69	1523.5
Qinghai	7.15	236.0	0.31	128.4	0.36	23.4	0.36	147.3	1.27	2948.9
Ningxia	14.34	523.8	1.96	129.6	1.06	16.6	1.14	478.6	2.95	3603.5
Sichuan	36.88	46.3	1.11	-43.2	3.20	7.4	1.66	8.1	4.54	1073.8
Chongqing	9.75	24.2	0.48	-69.2	1.11	4.6	0.26	-51.4	0.77	385.1
Guizhou	29.82	28.9	2.78	-8.6	2.13	68.9	1.99	60.3	3.26	739.0
Yunnan	35.65	129.2	1.70	15.5	1.96	32.2	1.52	56.9	2.49	728.5
Xizang	1.07	235.3	0.004	23.1	0.26	95.7	0.13	888.7	0.46	15960.2

References

Feng, S., Jiang, F., Jiang, Z., Wang, H., Cai, Z., and Zhang, L.: Impact of 3DVAR assimilation of surface PM2.5 observations on PM2.5 forecasts over China during wintertime, Atmospheric Environment, 187, 34-49, 2018.

Huang, X., Ding, A., Gao, J., Zheng, B., Zhou, D., Qi, X., Tang, R., Wang, J., Ren, C., Nie, W., Chi, X., Xu, Z., Chen, L., Li, Y., Che, F., Pang, N., Wang, H., Tong, D., Qin, W., Cheng, W., Liu, W., Fu, Q., Liu, B., Chai, F., Davis, S. J., Zhang, Q., and He, K.: Enhanced secondary pollution offset reduction of primary emissions during COVID-19 lockdown in China, National Science Review, doi: 10.1093/nsr/nwaa137, 2020. 2020.

Shi, X. and Brasseur, G. P.: The Response in Air Quality to the Reduction of Chinese Economic Activities During the COVID-19 Outbreak, 47, e2020GL088070, 2020.

Zhi, G., Zhang, Y., Sun, J., Cheng, M., Dang, H., Liu, S., Yang, J., Zhang, Y., Xue, Z., Li, S., and Meng, F.: Village energy survey reveals missing rural raw coal in northern China: Significance in science and policy, Environmental Pollution, 223, 705-712, 2017.